RESEARCH ARTICLE

Characterization of the tribologically relevant cover layers formed on copper in oxygen and oxygen-free conditions

Selina RAUMEL[1,*], **Khemais BARIENTI**[2], **Hoang-Thien LUU**[3], **Nina MERKERT**[3], **Folke DENCKER**[1], **Florian NÜRNBERGER**[2], **Hans Jürgen MAIER**[2], **Marc Christopher WURZ**[1]

[1] *Institute of Micro Production Technology, Leibniz Universität Hannover, Garbsen 30823, Germany*

[2] *Institut für Werkstoffkunde (Materials Science), Leibniz Universität Hannover, Garbsen 30823, Germany*

[3] *Institute of Applied Mechanics, Clausthal University of Technology, Clausthal-Zellerfeld 38678, Germany*

© The author(s) 2022.

Abstract: Engineering in vacuum or under a protective atmosphere permits the production of materials, wherever the absence of oxygen is an essential demand for a successful processing. However, very few studies have provided quantitative evidence of the effect of oxidized surfaces to tribological properties. In the current study on 99.99% pure copper, it is revealed that tribo-oxidation and the resulting increased abrasive wear can be suppressed by processing in an extreme high vacuum (XHV) adequate environment. The XHV adequate atmosphere was realized by using a silane-doped shielding gas (1.5 vol% SiH_4 in argon). To analyse the influence of the ambient atmosphere on the tribological and mechanical properties, a ball–disk tribometer and a nanoindenter were used in air, argon, and silane-doped argon atmosphere for temperatures up to 800 °C. Resistance measurements of the resulting coatings were carried out. To characterize the microstructures and the chemical compositions of the samples, the scanning electron microscopy (SEM), energy-dispersive X-ray spectroscopy (EDS), and X-ray diffraction (XRD) were used. The investigations have revealed a formation of η-Cu_3Si in silane-doped atmosphere at 300 °C, as well as various intermediate stages of copper silicides. At temperatures above 300 °C, the formation of γ-Cu_5Si were detected. The formation was linked to an increase in hardness from 1.95 to 5.44 GPa, while the Young's modulus increased by 46% to 178 GPa, with the significant reduction of the wear volume by a factor of 4.5 and the suppression of further oxidation and susceptibility of chemical wear. In addition, the relevant diffusion processes were identified using molecular dynamics (MD) simulations.

Keywords: wear behavior; tribochemical reaction; oxidation behavior; surface analysis; molecular dynamics (MD) simulation

1 Introduction

High wear is often observed during production processes under normal atmosphere in the metalworking industry, particularly due to surface oxidation on tools and parts. Accordingly, the focus of the present investigation is the question to what extent the wear mechanisms of samples processed in an extreme high vacuum (XHV)-adequate atmosphere, different from those in an air atmosphere. In order to characterize the basic effects of oxide formation and resulting wear mechanisms and to minimize additional influences, the oxygen-affine material copper was chosen in a copper/copper material pairing. Even though most of technically processed copper goes to the electrical industry (65%) and construction (25%) [1], however, the poor corrosion resistance of copper and the interaction with other process materials are of major

---

concern. Therefore, the oxidation behavior of copper has attracted interest and ongoing research focus on its effects on various processing properties [2–10]. At temperatures above 600 °C, oxidation is controlled by lattice diffusion. Here the copper ions diffuse through the Cu_2O layer [2, 11–13]. Below 500 °C, the reported kinetic data for oxidation vary considerably [9, 14]. A kinetic study on the oxidation over the temperature range from 350 to 1,050 °C has been performed by Zhukov [14]. Diffusion of oxygen from the surface into the bulk copper material at the grain boundaries is considered to be the critical factor for oxidation in a temperature range from 200 to 550 °C [7, 14]. At low temperatures, a part of the oxygen molecules are physically adsorbed. Dissociation of the oxygen molecules and diffusion only occurs at particularly energetic surface points [15]. This leads to an excessive wear resulting from tribo-oxidation due to tribo-induced oxidation by diffusion under load [16]. Since there are certain applications, such as cold welding, where the surface oxide content of the copper should be as low as possible to increase the forming capacity, there is a high research interest in oxygen-free production [17–19]. It is known that about 5 to 15 ppmv oxygen is still contained in technical grades of inert gases such as argon [20]. Even employing a high-purity inert gas (with approx. 0.05 ppmv oxygen) or ultrahigh vacuum (UHV) will not suppress the fast formation of an oxygen monolayer since according to the surface impact rate, a freshly exposed surface will still experience more than 1,018 collisions with oxygen molecules per square centimeter and second [21, 22]. For this reason, an XHV-adequate atmosphere was employed by means of a silane–argon mixture in the present study as proposed by Holländer et al. [23]. Using this oxygen concentrations of up to 10^{-24} bar (10^{-21} ppm) are achievable.

The scope of this study was to investigate the friction and wear behavior, as well as microstructural changes in the layers in an oxygen-free environment under XHV-adequate conditions with oxygen partial pressures of ~10^{-19} Pa (10^{-24} bar). In addition, the diffusion processes of the silicon were investigated in more detail by means of molecular dynamics (MD) simulation.

## 2   Materials and methodical approach

The XHV-adequate atmosphere was realized by doping argon (≤ 5 ppmv H_2O, ≤ 5 ppmv O_2, and ≤ 10 ppmv N_2) with 1.5 vol% SiH_4. Oxygen and water are eliminated from the atmosphere by Reactions (1) and (2) [24]:

$$SiH_4(g) + O_2(g) \rightarrow SiO_2(s) + 2H_2(g) \qquad (1)$$

$$SiH_4(g) + 2H_2O(g) \rightarrow SiO_2(s) + 4H_2(g) \qquad (2)$$
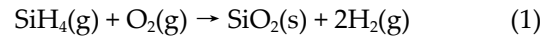
When adding a few parts per million by volume of SiH_4, the oxygen partial pressure will immediately decrease. Holländer et al. [23] and Lützenkirchen-Hecht et al. [25] showed that SiH_4 concentrations of 10^{-15} ppmv are sufficient to ensure extremely low oxygen levels. While using SiH_4, the achievable oxygen partial pressure is many orders of magnitude lower than that in technically producible ultra-high vacuum [20].

To investigate the wear behavior under XHV-adequate conditions, ball-on-disc investigations were carried out on a modified universal tribometer (UMT) (Fig. 1). For this experiment, disc-shaped samples (diameter = 50 mm, height = 10 mm) were manufactured from 99.99% pure copper round material. The surface was prepared by a grinding and polishing process to an average roughness (R_a) of less than 50 nm and an average roughness depth (R_z) of approx. 1 μm. The copper ball (diameter = 2 mm) was manufactured according to DIN 5401:2002-08 in a G500 quality [26]. Subsequently, the copper balls and the discs were characterized by means of nanoindentations (Ti 900, Hysitron) and the confocal microscopy. The characterization was carried out regarding their hardness (according to DIN EN ISO 14577-1), their Young's modulus (according to Oliver and Pharr), and their surface roughness (according to DIN EN ISO 25178) as well as their line roughness (according to DIN EN ISO 4287) [27–30]. For the nanoindentation, the force was applied within 5 s, after which, the force was held for 2 s and released for 5 s.

The indentation forces were set in ranges from 100 to 1,000 μN. The electrical resistance was investigated *in situ* by means of a specially manufactured four-point measuring system.
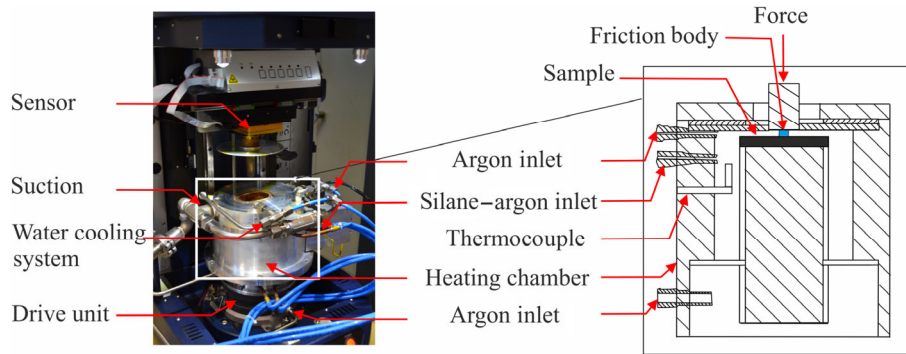
Fig. 1 Picture and schematic representation of universal tribometer with overpressure high temperature chamber.

2.1 Surface analysis

To characterize the microstructures and the chemical compositions of the samples, the scanning electron microscopy (SEM) and energy-dispersive X-ray spectroscopy (EDS) were used. The techniques were supplemented by the X-ray diffraction (XRD) to identify the phase composition of the near-surface layers. Polished cross sections were produced for the investigations. For this purpose, the specimens were cut and embedded. The surface was polished and cleaned afterwards. For the SEM/EDS measurements, a system (LEO 1455VP, Zeiss) was used. The SEM and EDS were performed under high vacuum conditions at a system base pressure of 10^{-4} Pa (10^{-6} mbar). The SEM images of the sample surface were taken at an acceleration voltage of 15–20 kV and a probe current of 0.7 nA. The EDS measurements were carried out at 15 kV and 1.4 nA using a recurrent. The XRD measurements were performed using an X-ray diffractometer (D8 Discover, Bruker) and a two-dimensional (2D) area detector (500, Vantec) using a Co Kα radiation. The step size during the measurement was 20°, and the measurement was performed according to the symmetrical 2θ scan method. During the measurement, the samples were rotated around Φ = 360 (°)/min to improve the measurement quality.

2.2 Tribology process

To assess the influence of the XHV-adequate environment, tests were also carried out in air as well as in argon atmosphere as a reference. To determine the frictional behavior at the contact interface, a UMT (TriboLab, Bruker) with an additional self-modified

high temperature cell (Fig. 1) was used according to the ASTM G99-17 test standard [31].

The argon, doped with 1.5 vol% SiH$_4$, was introduced into the resulting intermediate space between the ball and the disc sample through an additionally added gas inlet with a gas flow rate of 4 sL/min (cf. Fig. 1). A constant flow of argon (6 sL/min) at the top and bottom ensured that a slight overpressure inside the housing of the heating chamber was maintained to prevent the surrounding air from reaching the sample. The oxygen partial pressure in the chamber was measured constantly by means of a λ-probe (L-probe EM 2020, Mesa GmbH) directly above the friction contact with 1.5 Hz and enables a targeted gassing of the chamber up to the desired oxygen partial pressure of 10^{-19} Pa. The 2 mm copper ball was pressed onto the rotating copper surface with a force of 2 N resulting in a surface pressure of 1.19 GPa (Hertzian pressure). The resulted reference contact area of 0.0084 mm^2 (standard deviation (σ) = 0.0016) was determined by measurements of wear scars at room temperature (RT) in normal atmosphere. The specimen was driven by a motor, while the ball was firmly clamped in the ball holder to avoid possible rolling friction. The sliding distance was set to 160 mm (approx. 1.3 revolutions) with a sliding speed of 62.8 mm/min in all tests. Before each friction test, one rotation was performed to mechanically remove any native oxide layer and to compensate for surface irregularities. The kinetic coefficient of friction (CoF, μ) was determined by Eq. (3):

$$\mu = \frac{F_f}{F_N} \qquad (3)$$

where the force of friction (tangential force (F_f)) was measured by the high-performance force sensors

of the UMT Tribolab at 100 Hz, and the normal force (F_N) was set for each experiment (2 N). The CoF was determined as an average value of approx. 13,500 measuring points, excluding the measured values during the transition of static friction to sliding friction to ensure the results with zero tangential force at zero applied load. In advance, the effect of adhesion on the CoF was investigated by preliminary ball-on-disc tests at 1, 2, and 4 N. The results of these tests showed that no dependence of the CoF on the F_N was observed when excluding the static friction.

The experiments were carried out in different atmospheres and temperature ranging from RT to 800 °C using a heating rate of 100 K/min followed by a 4 min rest plateau to ensure homogeneous and reproducible heating. The temperature was measured with an integrated thermocouple (SR630, Stanford) close to the sample (Fig. 1). The oxygen partial pressure in the chamber was measured constantly by means of a λ-probe (Mesa GmbH) directly above the friction contact. Still, dust formation (SiO_2) could be observed in the chamber corresponding to Reactions (1) and (2). Six replicates were performed for each temperature and atmosphere. For each temperature, the samples were first exposed to the temperature in the respective atmosphere, and after reaching the target temperature and the defined holding time, the ball-on-disc tests began in order to create a reproducible test environment. After completion of the ball-on-disc experiments, the sample was cooled in the respective atmosphere and finally removed and analyzed. For the geometrical measurements of the friction tracks, the three-dimensional (3D) profilometry (LK-H052, Keyence), confocal laser scanning microscopy (VK9700, Keyence), automated

optical inspection (AOI; Toolinspect, Confovis GmbH), 3D Metrology (Toolinspect, Confovis GmbH), and an analytical semi micro precision scale (Cubis, Satorius AG) were used to determine the wear volumes and roughness of the samples. To measure the wear scar depth, a 3D profilometry instrument (LK-H052, Keyence) was used, while the depth and width of the wear tracks were measured using the confocal microscope (VK9700, Keyence). The cross-sectional profiles of the wear scar were measured at six different points on the radial wear track (Fig. 2(a)), and then an average value of the measurements was calculated.

For the calculation of the cross-sectional area of the wear track (W_q) [32], Eq. (4) was used.

$$W_q = R'^2 \arcsin\left(\frac{d_\perp}{2R'}\right) - \frac{1}{2}R'd_\perp\sqrt{1-\left(\frac{d_\perp}{2R'}\right)^2} \qquad (4)$$

where R' is the fitted circumference with the radius of the curvature, and $d_\perp$ is the track width. Since all necessary parameters are known (Fig. 2(b)), the wear volume (W_V) is calculated by Eq. (5) [32]:

$$W_V = \frac{1}{3}\pi W_l^2(3R' - W_l) + W_q\Delta x \approx \frac{\pi d_\perp^4}{64R'} + W_q\Delta x \qquad (5)$$

where W_l is the complete linear wear, and Δx is the stroke. An error in the determination of R' due to the surface roughness (Fig. 2(b)) may occur. However, the deviations of the individual measurements per wear track were examined and can be neglected with 0.3%–0.5% according to Ref. [32].

The volume loss of the ball was measured by using 3D Metrology (Confovis) and comparing the images after the tests with the reference images of the virgin ball. Furthermore, the mechanical properties of the
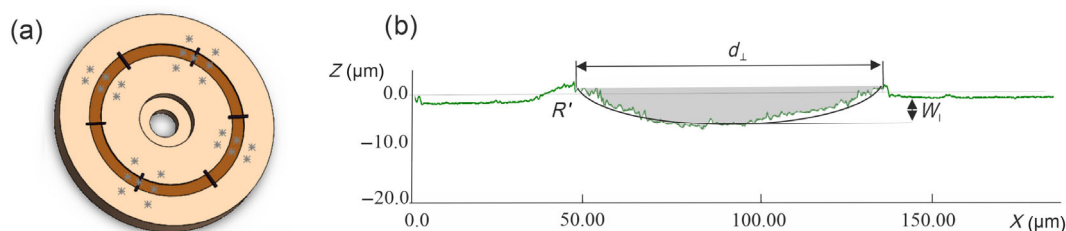
Fig. 2 (a) Illustration of the copper disc with one wear track and six positions for the wear volume observations (black) and the positions for the indentations (grey). (b) Exemplary line profile of a wear track measured by the laser scanning microscopy taken for the wear volume calculation. The planimetric wear as cross-sectional area of the wear track (W_q) is filled in gray. R' is the fitted circumference with the radius of the curvature, $d_\perp$ is the track width, and the complete linear wear is shown as W_l.

copper samples were measured using a triboindenter (TI900, Hysitron) with a Berkovich diamond tip (radius = 120 nm) on 26 positions (Fig. 2). The hardness was determined via plastic and elastic deformation. From the unloading curve of the recorded force–penetration curve, the hardness of the material under investigation was determined according to the method of Oliver and Pharr [28]. The modulus of elasticity results from the slope of the unloading curve after reaching the maximum indentation force. The surface roughness was investigated by means of an atomic force microscopy (AFM) scan [33]. For further resistance measurements, an insert for the UMT was made of ceramic with four integrated spring contact tips (pogo pins), which were connected to the universal measuring amplifier module (QuatumX MX840B, HBM) using four-wire technology.

2.3   Simulation setup

Classical MD simulation is a powerful method to investigate mechanical phenomena at the atomic scale. The method has been used to study a number of problems including the interaction of two surfaces during sliding [34] and adhesive wear mechanisms at the nanoscale [35]. Vakis et al. [36] reviewed the use of MD simulations for tribology and their role in cross-scale simulations.

Thus, we employed the MD method to predict interaction predictions of O_2 and SiH_4. It helped shed light on the elimination of oxygen molecules and their relationship to silicide formation on the Cu surface. To be able to study this process, MD simulations were used. In general, the positions, velocities, and energies of atoms (molecules) are calculated on the basis of a so-called interatomic potential. For decades, this method has been used to successfully simulate complex real-world phenomena, such as self-diffusion of n-alkanes in silicalite [37], plasticity and phase transformation in iron under high pressures [38], and the influence of oxidation on the behavior of aluminum nanostructures in uniaxial tests [39, 40]. In the present study, the variable-charge interatomic potential reactive force field (ReaxFF) was employed [41]. The scheme allows studying chemical reactions at the atomic scale. Bond formation and breakage

during the simulation process can be predicted precisely with lower computational cost compared to traditional density functional theory (DFT) calculations [42]. The potential was developed by combining and expanding previously tested and published ReaxFF force fields for Si/Al/O/H systems [43] and Cu/O/H systems [44]. The Cu/O/H force field reproduces the copper metal/metal and oxide/metal condensed phases [44], and the Si/O/H parameters successfully describe reactions of organics with Si and SiO_2 systems [43]. The stability of the ReaxFF potential [41] for simulating the SiH_4 atmosphere, the O_2 atmosphere, and Cu single crystals was tested at the beginning. The SiH_4 atmosphere, O_2 atmosphere, and single-crystal Cu were modeled separately. Based on the space group of molecules SiH_4 and O_2 in the gas, single molecules were first generated, and then replicated in all directions. As a result, 472 O_2 molecules and 135 SiH_4 molecules were created in a box with a size of 134 Å × 134 Å × 131 Å. The gas box is placed on top of a Cu(100) single crystal, having a dimension of 134 Å × 134 Å × 30 Å. The dimension of the simulation box including the Cu single crystal and atmosphere was 134 Å × 134 Å × 151 Å.

For relaxation, an NPT ensemble was used during 50 ps with a time step of 1 fs. The initial SiH_4, O_2 molecules, and Cu single crystal are stable during the relaxation process. The equilibrium bond length between the two oxygen atoms at 727 °C is in the range of 1.22–1.28 Å. The bond length between Si and H atoms during the relaxation is between 1.25 and 1.55 Å.

After the relaxation process, Cu(100) and Cu(100) covered with a thin oxide on the surface were exposed to the SiH_4 atmosphere. The simulations were performed in the NVT ensemble for 100 ps with periodic boundary conditions in *x*, *y*, and *z* directions. The temperatures were set to 727 °C with a damping constant that is 100 times the time step. Simulations in this study were carried out by the large-scale atomic/molecular massively parallel simulator (LAMMPS) [45]. It is open-source code and is widely used by the computational material science community. The OVITO Pro [46] was employed for the visualization and analysis of atomic simulation data generated by LAMMPS.

3   Results

3.1   Mechanical properties

From the optical observation of the samples (Fig. 3(a)), it is evident that the atmospheres have a significant influence on the interface formation dependent on the temperature. Significant differences in the discoloration of the surfaces are visible. The samples heat treated in normal atmosphere show a typical dull brown discoloration due to the thermal oxidation of copper and additionally a partial detachment of the upper layer. While the samples tested in silane–argon atmosphere show two different surfaces, on the main part, the typical shiny red–golden surface of copper is seen along with additionally shiny silver spots, and the sample probed in argon atmosphere shows a change by temperature from shiny gold (400 °C) to a dull brown (800 °C). Different surface formation was also visible considering the roughness. Before the start of the tests, the polished specimens had a surface roughness (R_a) of 0.04 μm and a R_z of 1.01 μm measured by the confocal microscopy. After the tests, under air atmosphere at 800 °C, the samples had a R_a of 0.29 μm and a R_z of 4.28 μm. The specimens in silane–argon atmosphere showed significantly lower roughness values with R_a = 0.06 μm and R_z = 1.61 μm.

The Young's modulus in normal atmosphere decreases significantly by 69% from 122 GPa at RT to 38 GPa at 800 °C, and that in argon atmosphere decreases by 66% from 122 GPa (RT) to 42 GPa (800 °C). In contrast, the Young's modulus in silane–argon atmosphere increases by about 46% from 122 to 178 GPa (cf. Fig. 3(b)).

The electrical resistance of the initial sample before the experiments showed a resistance of 0.21 Ω. The sample in normal atmosphere showed a positive correlation between increasing temperature and resistance up to 1.62 MΩ at 800 °C with a significant increase from 400 °C (31.56 kΩ). In silane–argon atmosphere, there was hardly any change in electrical resistance. A slight increase was seen up to about 200 °C to 4.65 Ω, but this value subsequently for higher temperatures dropped to < 1 Ω (800 °C at 0.32 Ω).

3.2   Wear and friction

The wear volume investigations showed a correlation of the changed hardness and the wear volume (cf. Fig. 4). It became visible that the wear volume in normal atmosphere increased sharply above 500 °C from approx. 54×10^{-3} to 147×10^{-3} mm³, while only a minimal increase in wear volume by 9×10^{-3} mm³ was detectable in silane–argon atmosphere. The wear volume in silane–argon atmosphere increased from 37×10^{-3} mm³ (RT) to 46×10^{-3} mm³ (500 °C).

Above 500 °C, the rate of increase of the wear volume as a function of temperature is much smaller in silane–argon atmosphere compared to that in the air or argon atmosphere, while the hardness increased drastically from 600 to 800 °C (2.4 GPa (σ = 0.03) to 5.44 GPa (σ = 0.11)) (cf. Fig. 4(b)). In comparison, the hardness decreased from 1.95 GPa (σ = 0.04) to 1.73 GPa (σ = 0.02) in normal atmosphere and increased up to 2.2 GPa (σ = 0.08) in argon atmosphere.
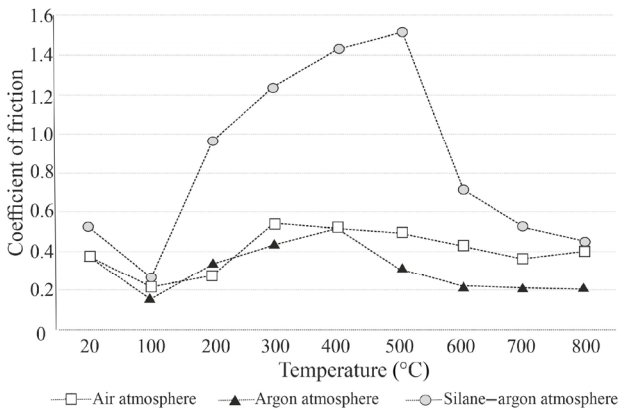
An increase of the CoF in a silane–argon atmosphere from 0.3 (100 °C) to 1.5 (500 °C) is evident (cf. Fig. 5). From about 500 °C, the CoF decreases again. In air and argon atmospheres, there was a slight increase
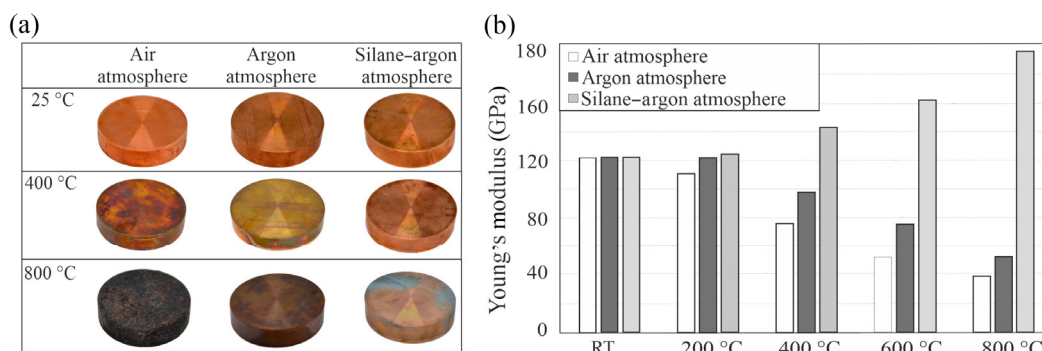
Fig. 3   (a) Visible changes of copper samples at RT (25 °C) and after a heat treatment (400 and 800 °C) in air, argon, and silane–argon atmosphere; (b) changes of the surface Young's modulus measured by indentations in dependence of temperature and atmosphere.
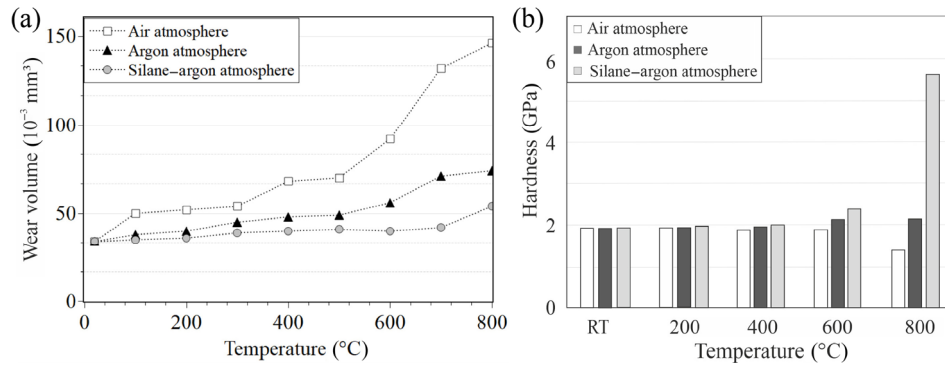
Fig. 4 (a) Calculated resulting wear volumes using the analyzed friction marks and (b) hardness of the copper disc samples as a function of temperature.

Fig. 5 CoFs of the samples in air, argon, and silane–argon atmosphere in ball-on-disc copper on copper testing as a function of temperature.

from 100 to 300 °C, which trended to level off again up to 800 °C. The increased roughness obtained in normal atmosphere was also evident in the results of the friction tests. The evaluation of the CoF showed increased σ in the curves in normal atmosphere starting from 400 °C. While the σ at 100 °C was 0.02, it changed up to $\sigma = 0.09$ at 800 °C.

Using the XRD analysis, the samples were examined in more detail at 100, 200, and 600 °C to investigate the reasons for the strong changes in the CoF. It was found that a slight native oxide layer was still visible at 100 °C. At 200 °C, the previous native oxide layer could no longer be detected, and from 600° onwards, there were clear silicon formation.

3.3 Surface analysis

As expected, a relatively thick oxide layer of about 10 µm could be measured on the surface of the sample in air atmosphere after being exposed to 800 °C for

30 min (cf. Fig. 6). The sample still consists essentially of copper but has a distinct excess layer of oxygen at the surface. The sample, which was tested in argon atmosphere, shows a slightly thinner oxide layer of about 2 µm. The sample tested in a silane–argon atmosphere, however, behaves differently. No additional layer can be identified on the basis of the image taken with the SEM. In the element distribution, it becomes apparent that no significant silicon-containing layer has formed on the surface but instead silicon diffused to the sample (2.54 wt%). Oxygen-containing layers
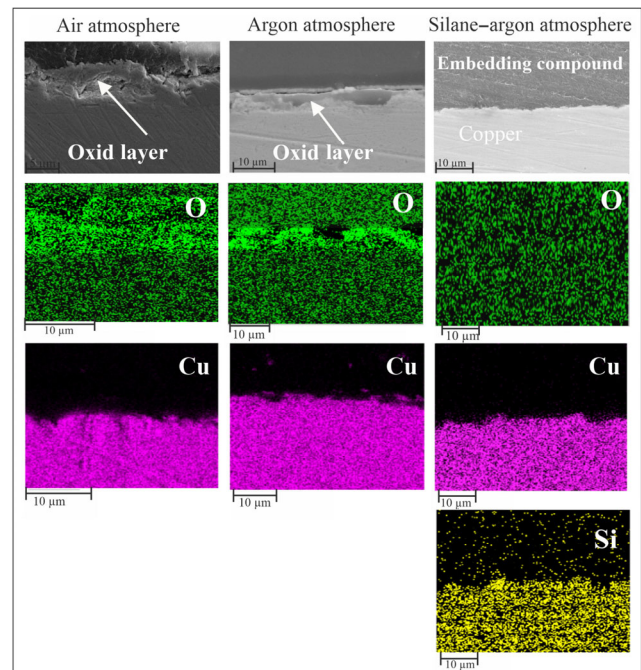
Fig. 6 SEM and EDS analysis of samples tested in various environments: The sample tested in air atmosphere shows a clear oxide layer, while no additional layer could be detected in the silane–argon sample.

or other indications of oxidation cannot be detected (cf. Fig. 6). The oxygen visible in the EDS analyse is from oxygen contamination due to the sample transport.

Both adhesive and abrasive wear could be detected during the examination of the ball. The 3D profilometry buildup and impressions of the surface were clearly visible probably due to a transfer from the disc or adhesion of wear debris during the friction tests.

The SEM images confirmed deposits due to adhesive processes. According to the EDS examinations, Si deposits were found on the sphere (10.45 wt%). Using the differential measurement modes of 3D Metrology, the maximum deviation of the sphere below the reference surface could be detected with an average of 78 μm and the maximum deviation above the reference surface with 24.5 μm.

Superficial observation of the sample in silane–argon atmosphere revealed two different surfaces. The pitting zone (cf. Fig. 7) is further investigated by the SEM and EDS analysis and found to be silicon accumulations. When the resulting layers were examined by the XRD, the results of the EDS investigations were confirmed. Figure 8 shows the XRD patterns of the samples processed in air atmosphere, argon, and silane–argon at 800 °C. It should be noted that two different measuring points are shown for the silane–argon sample. MP1 was recorded on the metallic clean surface, whereas MP2 describes the phase composition of the visually darker parts of the surface, as depicted in Fig. 7.

In accord with the SEM results (Fig. 6), a strong surface oxidation is observed, especially for the sample treated without a protective atmosphere. From the XRD data, the oxide layer formed consists mainly of copper(I) oxide (PDF 01-071-3645) [47] as well as small amounts of copper(II) oxide (PDF 00-001-1117) [47]. Based on the recorded spottiness in the raw

detector data, coarse polycrystalline oxides should be present. For the sample treated under argon, in addition to the underlying pure copper matrix, the formation of small amounts of copper(I) oxide on the sample surface is detected (PDF 01-071-3645 [47]). This finding is also consistent with the EDS results of the qualitative oxygen determination, as shown in Fig. 6. Compared to the sample treated at 800 °C without a protective atmosphere, a similar random morphology can be inferred for the oxide components formed based on the detector raw data. According to Zhou and Yang [13], the resulting morphology of copper(I) oxide is particularly dependent on the kinetics and thermodynamic conditions of formation caused by, e.g., the formation temperature or the oxygen partial pressure [48]. The samples treated under silane–argon featured an apparent differentiation of two surface areas into a metallic pure copper (MP1) and a pitting-zone (MP2) (cf. Fig. 7). On the metallic surface (MP1), in addition to the cubic copper matrix, only small amounts of η-Cu_3Si are detectable by the XRD. This is in contrast to the pitting areas (MP2), where a clear identification of various intermediate stages of the formation of copper silicides as well as small traces of SiO_2 is possible. Thermal exposure to a silane atmosphere leads to the formation of various silicides on the surface of the pure copper. These form over several reaction steps and can, in the worst case, precipitate to a brittle layer. As the temperature rises, the silicides change their composition and pass through several intermediate chemical steps. Thus, initially η-Cu_3Si (PDF 01-076-7859 [47]) is formed. At temperatures above 300 °C, γ-Cu_5Si (PDF 00-004-0841 [47]) and ε-$Cu_{15}Si_4$ (PDF 03-065-3166 [47]) grow on top of it. Consuming the copper 340 bound as η silicide, it can lead to the separation of the individual silicide layers when locally lower-lying η-Cu_3Si is subsequently formed again [3].
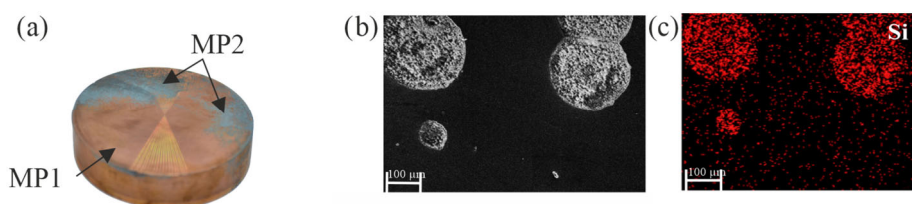
Fig. 7 (a) Copper sample treated under Silane–argon atmosphere showing two different surface areas: MP1—metallic pure copper and MP2—pitting zone. (b) SEM and (c) EDS analysis of Si deposits on Cu sample.
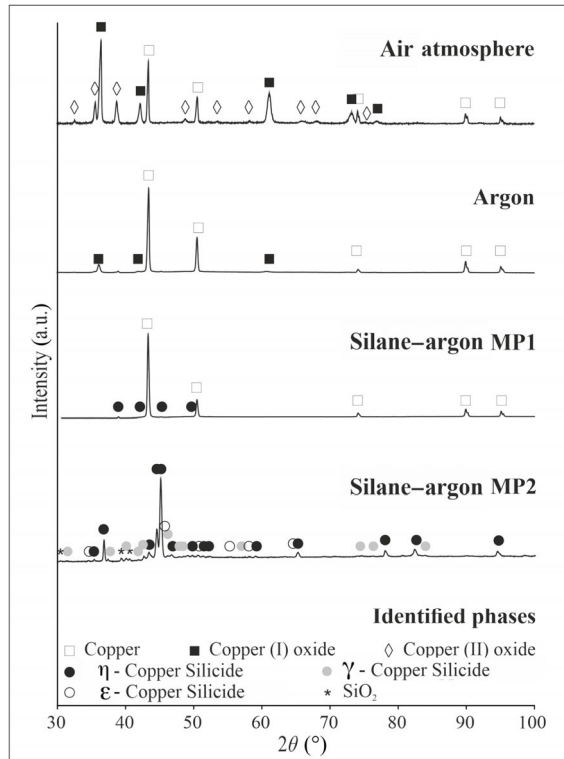
Fig. 8 XRD patterns for samples treated at 800 °C without protective atmosphere, in argon atmosphere, as well as in silane–argon atmosphere.

In addition, traces of SiO_2 (PDF 00-001-0649 [47]) can be detected, which can form as a thin surface film during the subsequent transport at normal atmosphere without significant temperature influence [3]. Hymes [3] also discovered that the silane exposure of copper samples at elevated temperatures will lead to the formation of γ-Cu_5Si, as the Cu_3Si is not stable in the presence of the underlying copper. The formation of the individual copper silicides is primarily controlled by diffusion processes. In particular, the formation of ε-$Cu_{15}Si_4$ is often kinematically inhibited in this way, and thus strongly dependent on atmospheric and processing conditions [3, 49].

Since it is of interest whether the silicon is diffusing into the sample origin from the silane in the atmosphere or from the reaction product of the silane with oxygen (SiO_2 particles), MD simulations were carried out to further investigate the influence of the silane atmosphere employed.

3.4　Surface silicide formation

MD simulations were carried out to investigate the influence of the oxygen atmosphere. The simulations show evidences that the Si atoms formed by the SiH_4 and O_2 reaction process play an important role in the formation of copper silicides at the surface. For further investigations about the influence of the oxide on the copper surface on the formation of sidicide and to accelerate the process, the deposition process of Si on Cu and Cu oxide surface was simulated. The relaxed structures of O_2, SiH_4, and Cu(100) surfaces are shown in Fig. 9. At 727 °C, the mean bond lengths of O_2 and SiH_4 are 1.25 and 1.40 Å, respectively. With the same reactive force field, the Cu crystal at 727 °C has a lattice constant of 3.72 Å. The oxidation process on Cu(100) was studied, and then the same Cu sample was placed under silane atmosphere and an mixture of silane and oxygen. The simulation result shows rapid chemisorption of oxygen on Cu(100) due to oxygen coalescence on the surface. The bond was broken, and the molecule dissociated into two atoms.

An oxide layer is quickly formed on the Cu surface (Video S1 in the Electronic Supplementary Material (ESM) for more details). Using the same procedure, the simulation of the Cu surface under silane atmosphere shows no evidence of direct adsorption or decomposition of SiH_4 on the substrate (Video S2 in the ESM). The result shows no direct adsorption of silane on Cu(100); the SiH_4 molecules collide with
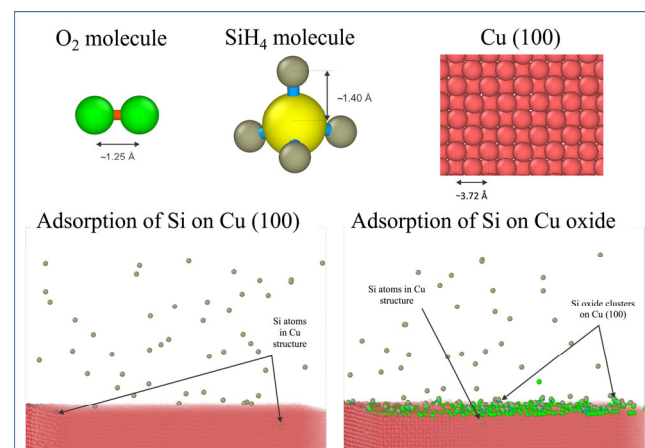
Fig. 9 Results from MD simulations. Bond lengths of O_2 molecule and SiH_4 and lattice constant of copper at 727 °C are shown in the first row. Details from snapshots of the Cu(100) after 17 ps on the bottom left, and Cu(100) oxide after 21 ps on the bottom right of deposition simulation at surfaces are shown (oxygen: green, hydrogen: brown, Si: yellow, and copper: red).

Cu(100) and bounce back. It is in agreement with the DFT calculation of the interaction of SiH_4 and Si surfaces [50]. To proceed the absorption of Si into Cu surface, SiH_4 must completely dissociates into SiH_x. The formation of surface silicides on metal surfaces has been reported in Refs. [50–53]. The adsorption and decomposition of SiH_4 depends on the SiH_4 concentration, crystal orientation [53], and mixture ratio between the silane and water/oxygen [51]. Thus, we placed Cu(100) single crystals under SiH_4–oxygen atmosphere. After 170 ps, a thin oxide layer formed on the Cu surface, and many species such as H_2O, SiH_x (x = 1, 2, and 3), and Si atoms (Video S3 in the ESM) were found. This suggests that the reaction of the silane with oxygen produces many intermediate compounds that could be associated with the silicide metal surface. The formation of the silicide copper surface is highly influenced by the surface quality and preparation [53]. To accelerate the simulation process of the formation of silicided Cu and to investigate the role of surface quality in the Si diffusion process, the experimental process of Graham et al. [54] was mimicked by depositing Si atoms on Cu(100) and Cu oxide surface. The results are shown in Fig. 9. Without the oxide layer, Si atoms drop onto the copper surface, and then diffuse into the sample. This result was also shown in the experimental tests since silicon was detected in the friction tracks, where the native oxide layer was mechanically removed. However, with the appearance of the oxide layer, the Si atoms interact with the Cu oxide. As a result, Cu–Si oxide is present on the surface. The oxide film acts as a diffusion barrier for Si, which means that Si requires more energy to diffuse into Cu compared to oxide-free surfaces. This finding is consistent with the result of Cabrera et al. [51] and Rebhan et al. [55], showing that oxide on steel prevents the diffusion of Si from the surface.

4   Discussion and concluding remarks

The XHV-adequate atmosphere causes a formation of copper–silicide, which results in considerable changes, especially in the mechanical properties of the material, the frictional forces resulting from sliding, and thus on the wear behavior of copper.

The different roughness measurements of the resulting surfaces by the confocal microscopy are due to the different layer development at high temperatures depending on the surrounding atmosphere. The lower roughness values of the sample in silane–argon atmosphere compared to those of the samples in normal atmosphere can be explained by the fact that the formation of the oxide layer was suppressed. Whereas in normal atmosphere, the results showed that the roughness of the samples increased after thermal oxidation, as shown in Refs. [56, 57]. This could also explain the comparatively low CoF up to 200 °C since Refs. [58, 59] suggest an influence of the roughness on the CoF, as a higher roughness can lead to a decreasing CoF, as stated by Sedlaček et al. [58] and Patel et al. [59].

Therefore, the results of the CoF in normal atmosphere can be explained by both the limited frictional contact of the two materials without direct contact of the copper surfaces due to the native oxide layer and the increased roughness. In addition, Chertavskikh and Kan [60] showed that the CoF decreases with the increasing heat of oxide layer formation, as is also the case in our experiments.

The increase in the CoF in normal atmosphere from 200 °C results from an increasing solidification of the oxide layer. It became clear that as soon as a critical thickness of the oxide layer is reached, the previously fallen CoF increases again. Chertavskikh and Kan [60] and Wilson et al. [61] obtained similar results, since a decrease in the CoF with the increasing thickness of the oxide layer applies only to thin oxide layers with adsorbed surfaces that increase the force of molecular interactions. Following Ref. [61], it was evident that if the oxide layer is thick enough, the porosity increases, and the hardness decreases.

In addition, Ref. [62] confirms that abrasion by porosity results from the acceleration of the diffusion rate of oxygen at elevated temperatures. Quinn [63] also observed in his experiments cracking on the oxide layer when it reaches a critical thickness of about 1–3 μm.

Another factor is the contribution of the adhesion tendency, which becomes crucial at higher temperatures due to the higher chemical activity of the bulk material.

Liu et al. [64] state that the essential process in the adhesion of Cu/Cu is found to be surface diffusion. Therefore, the samples in normal atmosphere show a lower CoF but an increased formation of wear particles. The initial reduction of the CoF in XHV-adequate atmosphere was shown to be due to the presence of the native oxide layer. The increase in the CoF detected between 100 and 500 °C can be explained by the mechanical removal and thermal deoxidation of the friction-reducing native oxide layers, which cannot reform due to the absence of oxygen.

As a result, direct frictional contact of the two materials takes place in dry contact and therefore an increase in the adhesion tendency. It was also shown that the removal of the sources of surface oxidation in high vacuum will lead to an increasing level of adhesion and therefore friction [4, 65, 66]. This can be explained by the electron transfer between the contacting surfaces [67, 68]. The adhesion as a result of the direct contact can also be identified visually on the ball and the wear mark. The abrupt reduction in the CoF at elevated temperatures (< 500 °C) can be explained by the formation of a hard tribologically relevant silicide layer in the reactive atmosphere. This layer also shows a favorable tribological behavior at temperatures up to 800 °C, which however, still exhibits a higher CoF than that in normal or argon atmosphere, which can be explained by the reduced surface roughness. The suppression of adhesion by increasing the hardness and elastic modulus of the newly formed surface layers is also reflected in the decreased CoF [69]. During the friction tests, both adhesion and the leveling of the asperities must have played a predominant role in determining the CoF.

The increase of the wear volume in air atmosphere from 29.2 to 127.08 μm^3 is explained by the increased tribochemical and abrasive wear due to the brittle oxide layers (mainly copper(I) oxide) formed on the surface. The drastic increase in the wear rate at elevated temperatures suggests that this form of wear is initially still metallic and from then on mainly oxidative wear [70]. Furthermore, the resulting deterioration of the mechanical properties due to the lattice distortion of the substrate can be explained by the adsorption-induced reduction in strength (Rehbinder effect) [71], which had an influence on the increased wear volume.

The elimination of oxidation processes and the associated suppression of tribochemical wear can explain the comparatively small increase in wear volume of only 9.8% in an atmosphere suitable for XHV.

Since no porous oxide layer is present, only limited removal of boundary layer particles is possible during adhesive processes. At the applied load and the sharp increase in hardness from 1.95 GPa at 25 °C to 5.44 GPa at 800 °C, there is hardly any cracking in the fusion zones or adjacent areas. Maier et al. [20] also stated that tribo-oxidation could be suppressed upon milling in an oxygen-free environment.

The increased hardness in XHV-adequate atmosphere can be explained by the silicides detected by the XRD and can be the reason for the reduction of adhesion wear [67]. In comparison, the slightly increased wear volume in argon atmosphere is related to the increased hardness and the only slightly formed and stable oxide layer. During the investigations, the temperatures between 400 and 550 °C proved to be particularly decisive. For this reason, further focus was placed on the temperature range from 400 °C upwards. The SEM and XRD examinations of the sample in argon atmosphere showed that even the smallest amounts of oxygen are sufficient to form stable oxide layers, especially at higher temperatures. This confirms the statement in Ref. [20] that in conventional inert gas atmospheres, there is a sufficient oxygen concentration to contaminate the surfaces.

The decrease of the elastic modulus in normal atmosphere is already known [72, 73]. By increasing the temperature, the atoms gain a significant amount of kinetic energy. Thus, as the temperature increases, the space between the individual particles becomes larger, reducing the interaction energy. As a result, the Young's modulus decreases with the increasing temperature in metal-bonded solids. The change of elastic modulus with temperature involves the atomic bonding force. This can also explain why the Young's modulus behaves differently in silane–argon atmosphere. The diffusion of Si into copper changes the atomic binding force, which leads to the increase in the Young's modulus and hardness. In addition, this may also have resulted in the filling of microcracks created by thermal expansion mismatch, reducing porosity and increasing elastic modulus and strength

[74] as solid solution strengthening of copper is a common process [75].

The EDS images suggest that SiO_2 accumulating on the surface is sintering. Using MD simulation, it could be shown that Si atoms diffuse into copper. In Ref. [76], it is known that the copper silicides provide oxygen resistance to the underlying copper. With the MD method using the ReaxFF potential, this complex process could be simulated. Oxygen molecules react rapidly with the Cu surface and form a thin oxide on the sample surface within a few picoseconds. SiH_4 has a weak binding with the Cu(100), similar to that with the Si(100) [50]. However, in the SiH_x (x = 1, 2, and 3), Si atoms show evidence of binding with the surface and later diffuse into the Cu(100). The reaction between Si–H compounds and oxide thin film on Cu surface happens within 1 ps. Therefore, it requires more energy and time for the adsorption of Si on the Cu surface.

The electrical resistance of the sample in normal atmosphere can be explained by the fact that during the formation phase, the contact resistance increases due to growing oxide layers. In Ref. [77], it was shown that already thin layers in the atomic range can have a significant influence on the contact resistance [77, 78]. An explanation for the only slightly changed electrical conductivity in silane–argon atmosphere could be that the basic resistance of the copper was measured by the prevented oxidation here. An increase in resistance due to the silicides could not be detected due to the size of the Cu sample. In the future, measurements with Cu foil in silane–argon atmosphere should be performed. Furthermore, the use of conductive atomic force microscopy (C-AFM) to test the morphology and conductivity synchronously should be considered. Since there were no changes in the resistivity of the silane–argon samples after several weeks and also after further thermal treatments in normal atmosphere, it can be assumed that the Cu–Si formation has a positive influence on the prevention of further oxidation of the underlying copper.

Hymes et al. [76] also showed in his experiments on the passivation of copper by means of silicide formation that in thermal experiments, the formed silicon containing layers will protect the copper from further corrosion in oxidizing atmosphere.

In summary, the investigations showed that the oxygen-free atmosphere has a significant influence on the tribological processes of copper. By reducing tribochemical wear, the wear volume in XHV-adequate atmosphere could be greatly reduced by a factor of 4.5 compared to the wear volume in air atmosphere in this setup. The increased CoF in silane–argon atmosphere up to 500 °C was subsequently reduced by the silicide formation. In addition, it can be assumed that the copper silicides formed in XHV-adequate atmosphere provide oxygen resistance to the underlying copper, which gives a clear advantage in post-metal processing in the production of silicon-integrated circuits. Significant potentials were shown due to the eliminated susceptibility of chemical wear and the improved mechanical properties.

Acknowledgements

Declaration of competing interest

The authors have no competing interests to declare that are relevant to the content of this article.

Data availability

The raw and processed data generated are available upon requests.

Electronic Supplementary Material Supplementary material is available in the online version of this article at https://doi.org/10.1007/s40544-022-0695-5.

References

[1] Bennett C. Meeting future copper demand. Available on https://copperalliance.org/resource/meeting-future-copper-demand/, 2019.

[2] Mrowec S, Stokłosa A. Oxidation of copper at high temperatures. *Oxid Met* **3**(3): 291–311 (1971)

[3] Hymes S W. Growth and stability of copper silicide thin films. Ph.D. Thesis. Ann Arbor (USA): Rensselaer Polytechnic Institute, 1999.

[4] Bowden F P, Tabor D. *The Friction and Lubrication of Solids*. Oxford (UK): Clarendon Press, 1986.

[5] Kragelski I W. *Reibung und Verschleiss*. München (Germany): Hanser, 1971. (in German)

[6] O'Reilly M, Jiang X, Beechinor J T, Lynch S, NíDheasuna C, Patterson J C, Crean G M. Investigation of the oxidation behaviour of thin film and bulk copper. *Appl Surf Sci* **91**(1–4): 152–156 (1995)

[7] Lee S K, Hsu H C, Tuan W H. Oxidation behavior of copper at a temperature below 300 °C and the methodology for passivation. *Mater Res* **19**(1): 51–56 (2016)

[8] Lehmann J S, Schwaiger R, Rinke M, Greiner C. How tribo-oxidation alters the tribological properties of copper and its oxides. *Adv Mater Inter* **8**(1): 2001673 (2021)

[9] Rau J S, Schmidt O, Schneider R, Debastiani R, Greiner C. Three regimes in the tribo-oxidation of high purity copper at temperatures of up to 150 °C. *Adv Eng Mater* **24**(11): 2200518 (2022)

[10] Unutulmazsoy Y, Cancellieri C, Chiodi M, Siol S, Lin L C, Jeurgens L P H. *In situ* oxidation studies of Cu thin films: Growth kinetics and oxide phase evolution. *J Appl Phys* **127**(6): 065101 (2020)

[11] Zhukov V, Popova I, Yates J T. Electron-stimulated oxidation of Al(111) by oxygen at low temperatures: Mechanism of enhanced oxidation kinetics. *Phys Rev B* **65**(19): 195409 (2002)

[12] Peng J, Chen B L, Wang Z C, Guo J, Wu B H, Hao S Q, Zhang Q H, Gu L, Zhou Q, Liu Z, et al. Surface coordination layer passivates oxidation of copper. *Nature* **586**(7829): 390–394 (2020)

[13] Zhou G W, Yang J C. Temperature effect on the Cu$_2$O oxide morphology created by oxidation of Cu(001) as investigated by *in situ* UHV TEM. *Appl Surf Sci* **210**(3–4): 165–170 (2003)

[14] Zhukov V P. Mathematical model of deoxidation of copper by solid carbon. *Metallurgist* **60**(7): 771–775 (2016)

[15] Katayama T, Sekiba D, Mukai K, Yamashita Y, Komori F, Yoshinobu J. Adsorption states and dissociation processes of oxygen molecules on Cu(100) at low temperature. *J Phys Chem C* **111**(41): 15059–15063 (2007)

[16] Rau J S, Balachandran S, Schneider R, Gumbsch P, Gault B, Greiner C. High diffusivity pathways govern massively enhanced oxidation during tribological sliding. *Acta Mater* **221**: 117353 (2021)

[17] Zhou H J, Wu W P, Wu R N, Hu G M, Xia R. Effects of various conditions in cold-welding of copper nanowires: A molecular dynamics study. *J Appl Phys* **122**(20): 204303 (2017)

[18] Steudel H. *Werkstoff-handbuch Nichteisenmetalle*. Düsseldorf (Germany): VDI-Verlag, 1960. (in German)

[19] Miyoshi K. Aerospace mechanisms and tribology technology: Case studies. In: NASA Glenn Research Center, Cleveland, USA, 1999, **7**: NASA/TM-107249.

[20] Maier H J, Herbst S, Denkena B, Dittrich M A, Schaper F, Worpenberg S, Gustus R, Maus-Friedrichs W. Towards dry machining of titanium-based alloys: A new approach using an oxygen-free environment. *Metals* **10**(9): 1161 (2020)

[21] Raumel S, Barienti K, Dencker F, Nürnberger F, Wurz M C. Einfluss von silan-dotierten umgebungsatmosphären auf tribologischen eigenschaften von titan. *Tribol und Schmierungstechnik*: https://doi.org/10.24053/TuS-2021-0002 (2021) (in German)

[22] Jousten K, Wutz M, Adam H, Walcher W. *Handbook of Vacuum Technology: Influence of Oxygen on the Tool Wear in Machining*, 12th edn. Weinheim (Germany): Springer Verlag Wiesbaden, 2008.

[23] Holländer U, Wulff D, Langohr A, Möhwald K, Maier H J. Brazing in SiH$_4$-doped inert gases: A new approach to an environment friendly production process. *Int J Pr Eng Man–GT* **7**: 1059–1071 (2020)

[24] Kroke E, Müller A. *Eigenschaften und Reaktionsverhalten von Silicium*, Ph.D. Thesis. Germany: Bergakademie Freiberg, 2017.

[25] Lützenkirchen-Hecht D, Wulff D, Wagner R, Frahm R, Holländer U, Maier H J. Thermal anti-oxidation treatment

of CrNi-steels as studied by EXAFS in reflection mode: The influence of monosilane additions in the gas atmosphere of a continuous annealing furnace. *J Mater Sci* **49**(15): 5454–5461 (2014)

[26] Deutsches Institut für Normung e.V. DIN 5401:2002-08 Wälzlager—Kugeln für wälzlager und allgemeinen Industriebedarf. DIN, 2002. (in German)

[27] Deutsches Institut für Normung e.V. DIN EN ISO 21920-2:2022: Geometrical product specifications (GPS)—Surface texture: Profile method—Terms, definitions and surface texture parameters. Beuth Verlag GmbH, 2022.

[28] Oliver W C, Pharr G M. An improved technique for determining hardness and elastic modulus using load and displacement sensing indentation experiments. *J Mater Res* **7**(6): 1564–1583 (1992)

[29] Deutsches Institut für Normung e.V. DIN EN ISO14577-1:2015 Metallische werkstoffe instrumentierte eindringprüfung zur bestimmung der härte und anderer werkstoffparameter DIN, 2015. (in German)

[30] Deutsches Institut für Normung e.V. DIN EN ISO 25178-1:2016 Geometrische produktspezifikation für oberflächenbeschaffenheit. DIN, 2016. (in German)

[31] US-ASTM. ASTM G99-17 Standard test method for wear testing with a pin-on-disk apparatus. ASTM, 2017.

[32] Reichelt M, Cappella B. Comparative analysis of error sources in the determination of wear volumes of oscillating ball-on-plane tests. *Frontiers in Mechanical Engineering* **6**: 25 (2020)

[33] Walker J, Umer J, Mohammadpour M, Theodossiades S, Bewsher S R, Offner G, Bansal H, Leighton M, Braunstingl M, Flesch H G. Asperity level characterization of abrasive wear using atomic force microscopy. *P Roy Soc A-Math Phy* **477**(2250): 20210103 (2021)

[34] Rigney D A, Karthikeyan S. The evolution of tribomaterial during sliding: A brief introduction. *Tribol Lett* **39**(1): 3–7 (2010)

[35] Aghababaei R, Warner D H, Molinari J F. Critical length scale controls adhesive wear mechanisms. *Nat Commun* **7**: 11816 (2016)

[36] Vakis A I, Yastrebov V A, Scheibert J, Nicola L, Dini D, Minfray C, Almqvist A, Paggi M, Lee S, Limbert G, et al. Modeling and simulation in tribology across scales: An overview. *Tribol Int* **125**: 169–199 (2018)

[37] Leroy F, Rousseau B, Fuchs A H. Self-diffusion of n-alkanes in silicalite using molecular dynamics simulation: A comparison between rigid and flexible frameworks. *Phys Chem Chem Phys* **6**(4): 775–783 (2004)

[38] Gunkelmann N, Bringa E M, Kang K, Ackland G J, Ruestes C J, Urbassek H M. Polycrystalline iron under compression: Plasticity and phase transitions. *Phys Rev B* **86**(14): 144111 (2012)

[39] Gunkelmann N, Bringa E M, Rosandi Y. Molecular dynamics simulations of aluminum foams under tension: Influence of oxidation. *J Phys Chem C* **122**(45): 26243–26250 (2018)

[40] Rosandi Y, Luu H T, Urbassek H M, Gunkelmann N. Molecular dynamics simulations of the mechanical behavior of alumina coated aluminum nanowires under tension and compression. *RSC Adv* **10**(24): 14353–14359 (2020)

[41] Psofogiannakis G M, McCleerey J F, Jaramillo E, van Duin A C T. ReaxFF reactive molecular dynamics simulation of the hydration of Cu–SSZ-13 zeolite and the formation of Cu dimers. *J Phys Chem C* **119**(12): 6678–6686 (2015)

[42] Paupitz R, Junkermeier C E, van Duin A C T, Branicio P S. Fullerenes generated from porous structures. *Phys Chem Chem Phys* **16**(46): 25515–25522 (2014)

[43] Van Duin A C T, Strachan A, Stewman S, Zhang Q S, Xu X, Goddard W A. ReaxFF$_{SiO}$ reactive force field for silicon and silicon oxide systems. *J Phys Chem A* **107**(19): 3803–3811 (2003)

[44] Van Duin A C T, Bryantsev V S, Diallo M S, Goddard W A, Rahaman O, Doren D J, Raymand D, Hermansson K. Development and validation of a ReaxFF reactive force field for Cu cation/water interactions and copper metal/metal oxide/metal hydroxide condensed phases. *J Phys Chem A* **114**(35): 9507–9514 (2010)

[45] Plimpton S. Fast parallel algorithms for short-range molecular dynamics. *J Comput Phys* **117**(1): 1–19 (1995)

[46] Stukowski A. Visualization and analysis of atomistic simulation data with OVITO—The Open Visualization Tool. *Model Simul Mater Sc* **18**(1): 015012 (2010)

[47] Gates-Rector S, Blanton T. The Powder Diffraction File: A quality materials characterization database. *Powder Diffr* **34**(4): 352–360 (2019)

[48] Luo L L, Kang Y H, Liu Z Y, Yang J C, Zhou G W. Effect of oxygen pressure on the initial oxidation behavior of Cu and Cu–Au alloys. *MRS Online Proc Libr* **1318**(1): 706 (2011)

[49] Sufryd K, Ponweiser N, Riani P, Richter K W, Cacciamani G. Experimental investigation of the Cu–Si phase diagram at x(Cu) > 0.72. *Intermetallics* **19**(10): 1479–1488 (2011)

[50] Spencer M J S, Nyberg G L, Robinson A W, Stampfl A P J. Adsorption of SiH$_4$ on copper (110) and (111) surfaces. *Surf Sci* **505**: 308–324 (2002)

[51] Cabrera A L, Kirner J F, Pierantozzi R. Si diffusion coating on steels by SiH$_4$/H$_2$ treatment for high temperature oxidation protection. *J Mater Res* **5**(1): 74–82 (1990)

[52] Cabrera A L, Kirner J F, Armor J N. Oxidation protection for a variety of transition metals and copper via surface silicides formed with silane containing atmospheres. *J Mater Res* **6**(1): 71–79 (1991)

[53] Chhun S, Gosset L G, Michelon J, Girault V, Vitiello J, Hopstaken M, Courtas S, Debauche C, Bancken P H L,

Gaillard N, et al. Cu surface treatment influence on Si adsorption properties of CuSiN self-aligned barriers for sub-65 nm technology node. *Microelectron Eng* **83**(11–12): 2094–2100 (2006)

[54] Graham A P, Hinch B J, Kochanski G P, McCash E M, Allison W. Two-dimensional silicide 5 × 3 structure on Cu(001) as seen by scanning tunneling microscopy and helium-atom scattering. *Phys Rev B* **50**(20): 15304–15315 (1994)

[55] Rebhan M, Meier R, Plagge A, Rohwerder M, Stratmann M. High temperature chemical vapor deposition of silicon on Fe(100). *Appl Surf Sci* **178**(1–4): 194–200 (2001)

[56] He L P, Cai Z B, Peng J F, Deng W L, Li Y, Yang L Y, Zhu M H. Effects of oxidation layer and roughness on the fretting wear behavior of copper under electrical contact. *Mater Res Express* **6**(12): 1265e3 (2019)

[57] Zheng Y T, Xuan F Z, Wang Z D. Surface roughness of the strained polycrystalline copper during the early stage oxidation. *Comput Mater Sci* **114**: 183–188 (2016)

[58] Sedlaček M, Podgornik B, Vižintin J. Influence of surface preparation on roughness parameters, friction and wear. *Wear* **266**(3–4): 482–487 (2009)

[59] Patel K, Doyle C S, Yonekura D, James B J. Effect of surface roughness parameters on thermally sprayed PEEK coatings. *Surf Coat Technol* **204**(21–22): 3567–3572 (2010)

[60] Chertavskikh A K, Kan K N. *Collection: Friction and Lubrication in the Machining of Nonferrous Metals*. Leningrad (Russia): Otdelenie tekhnicheskikh SSSR, 1945. (in Russian)

[61] Wilson J E, Stott F H, Wood G C. The development of wear-protective oxides and their influence on sliding friction. *P Roy Soc A-Math Phy* **369:** 557–574 (1980)

[62] Mimura K, Lim J W, Isshiki M, Zhu Y F, Jiang Q. Brief review of oxidation kinetics of copper at 350 °C to 1050 °C. *Metall Mater Trans A* **37**(4): 1231–1237 (2006)

[63] Quinn T F J. Review of oxidational wear. *Tribol Int* **16**(5): 257–271 (1983)

[64] Liu C M, Lin H W, Huang Y S, Chu Y C, Chen C, Lyu D R, Chen K N, Tu K N. Low-temperature direct copper-to-copper bonding enabled by creep on (111) surfaces of nanotwinned Cu. *Sci Rep* **5**: 9734 (2015)

[65] Buckley D H. *Surface Effects in Adhesion, Friction, Wear, and Lubrication*. Amsterdam (the Netherlands): Elsevier Amsterdam, 1981.

[66] Campbell W E, Thurber E A. Studies in boundary lubrication—II: Influence of adsorbed moisture films on coefficient of static friction between lubricated surfaces *Trans ASME* **70**(4): 401–406 (1948)

[67] Adhesion and adhesive wear. In: *Engineering TriBology*. Stachowiak G W, Batchelor A W, Eds. Amsterdam (the Netherlands): Butterworth–Heinemann, 1993: 613–635.

[68] Ziman J M. *Electrons in Metals: A Short Guide to the Fermi Surface*. London (UK): Taylor & Francis, 1963.

[69] Sikorski M E. The adhesion of metals and factors that influence it. *Wear* **7**:144–162 (1964)

[70] Gale W F, Totemeier T C. *Smithells Metals Reference Book*, 8th edn. Burlington (USA): Elsevier Butterworth–Heinemann, 2004.

[71] Andrade E N D C, Randall R F Y. The rehbinder effect. *Nature* **164**(4183): 1127 (1949)

[72] Youssef T H, Essawi R A. Effect of working temperature on Young's modulus of electrolytic copper. *Czech J Phys* **29**(11): 1266–1270 (1979)

[73] Li W G, Wang R Z, Li D Y, Fang D N. A model of temperature-dependent young's modulus for ultrahigh temperature ceramics. *Phys Res Int* **2011**: 1–3 (2011)

[74] Rand B. Composites: Carbon matrix. In: *Encyclopedia of Condensed Matter Physics*. Elsevier Ltd., 2005: 178–192.

[75] Maki K, Ito Y, Matsunaga H, Mori H. Solid-solution copper alloys with high strength and high electrical conductivity. *Scripta Mater* **68**(10): 777–780 (2013)

[76] Hymes S, Murarka S P, Shepard C, Lanford W A. Passivation of copper by silicide formation in dilute silane. *J Appl Phys* **71**(9): 4623–4625 (1992)

[77] Stephan S. Stromführende verbindungen und leiterwerkstoffe der elektroenergietechnik: Theorie zum kontakt-und langzeitverhalten von schraubenverbindungen mit Flächenkontakten. Dresden (Germany): Technischen Universität Dresden, 2019. (in German)

[78] Holm R. *Electric Contacts: Theory and Applications*, 4th edn. Berlin: Springer Berlin Heidelberg, 2000.

Selina RAUMEL. She received her bachelor's (2015) and master's degrees (2017) from University of Applied Sciences Kiel, Germany. In 2017, she started as a Ph.D. student at the Institute of Micro Production Technology (IMPT) at Leibniz Universität Hannover, Germany. Her research interests include microtribology and the mechanical and tribological analysis of thin films.

Khemais BARIENTI. He received his bachelor's and master's degrees in materials engineering from RWTH Aachen University, Germany, in 2014 and 2017, respectively. He then joined the Institute of Materials Science at Leibniz Universität Hannover, Germany, as a Ph.D. student. His research interests include cold roll bonding of sheet metal and XRD analysis.

Hoang-Thien LUU. He has achieved his Ph.D. degree from TU Clausthal, Germany, in 2022. Micromechanical and scale-bridging modeling of plastic deformation, crystal plasticity methods and parameter identification, and metal wear are areas of study interest for him.

Nina MERKERT (Née GUNKELMANN). She has been awarded a doctor of natural sciences. at TU Kaiserslautern, Germany. She is a junior professor for computational material sciences/engineering at TU Clausthal, Germany. Her fields of interest include molecular dynamics simulations and discrete element simulations of heterogeneous materials, as well as characterization of dislocation structures and plasticity utilizing multiscale techniques.

Folke DENCKER. He is a lecturer and researcher of nanotechnology at Leibniz University of Hannover at the Institute of Microproduction Technology (IMPT), Germany. With his background in tribology and sensor development, his principal research objective is the data acquisition in harsh environments.

Florian NÜRNBERGER. He received his Ph.D. degree in mechanical engineering from Leibniz Universität Hannover, Germany, in 2010. He then joined the Institute of Materials Science at Leibniz Universität Hannover, Germany. He is a senior researcher and his research areas include the heat treatment of metals, tailored forming technologies, and microstructure analysis.

Hans Jürgen MAIER. He received his Ph.D. degree in engineering from FAU Erlangen-Nuremberg, Germany, in 1990. He was then a professor at University of Paderborn, Germany. Since 2012, he has been a professor at Leibniz Universität Hannover, Germany, and director of the Institute of Materials Science, Germany. His research areas are process–microstructure–property relationships, investigation of mechanical properties and modern metal alloys.

Marc Christopher WURZ. He received his bachelor's degree at Leibniz Universität Hannover, Germany, in 2002. In 2003, he started his Ph.D. at the Institute of Micro Production Technology (IMPT) of the Leibniz Universität Hannover, Germany, and finished his thesis in 2009. Since October 2022, he is the director of IMPT. His research activities include magnetic sensors and actuators, new techniques for integrated circuits, and the application of microsystems in tools including new process technologies for microsystems. He has published his results in more than 150 publications. In addition, he has filed more than 20 patent applications.